

Soil Strength-based Estimation of Optimal Control Parameters for Wheeled Robots on Rough Terrain

Jayoung Kim and Jihong Lee

Dept. Of Mechatronics Engineering, Chungnam National University, Gungdong, Daejeon, Korea

Keywords: Optimal Control Parameter, Maximum Traction Coefficient, Optimal Slip Ratio, Tractive Efficiency, Soil Strength, Vehicle Dynamics, State Observer, Soil Identification, Wheeled Robot, Rough Terrain.

Abstract: On rough terrain, there are a variety of soil types having different soil strength. It means that it is needed for outdoor robots to change wheel control strategies since optimal slip and maximum traction levels on wheels differ depending on soil strength. Therefore this paper proposes an algorithm for acquiring optimal control parameters, such as maximum traction coefficient and optimal slip ratio to maximize traction or minimize energy consumption, based on estimating strength of soils. In this paper the optimal models of wheel traction and slip are derived through indoor experiments by a testbed for analysis of wheel-terrain interactions on three types of soil; grass, gravel and sand. For estimating soil strength, actual traction coefficient, including information of motion resistance, is observed by a state estimator related to wheeled robot dynamics. The actual traction coefficient and slip ratio on wheels are employed to estimate soil strength by a numerical method on the basis of derived optimal models. The proposed algorithm was verified through real driving experiments of a wheeled robot on various types of soil.

1 INTRODUCTION

Outdoor wheeled robots have overcome obstructions of moving on rough terrains, such as a slippery surface or a steep slope, in order to fulfil important tasks regarding the purpose of exploration, reconnaissance, rescue, etc. For achieving such goals, wheeled robots should have abilities to handle two kinds of characteristic changes on rough terrains; a change of soil types (slippery or non-slippery) and surface shapes (flat or steep). Both the terrain characteristic changes are crucial factors in the decision regarding optimal wheel slip or traction as a control parameter of a wheel controller since tractive force of a wheel is differently exerted on a surface according to such changes (Terry et al., 2008, Krebs et al., 2010, Joo et al., 2013, Ding et al., 2010, Ishigami et al., 2008, Brooks et al., 2012). In case of changing surface shapes, it is relatively easy for wheeled robots to realize the level of the change by motion sensors like inertial measurement units (IMU). On the contrary to this, it is not such an easy undertaking to judge a type of soil where a robot is operated in spite of using various sensors mounted on a robot. To solve this issue, many researches

related to soil identification have been introduced in the field of robotics.

The studies on soil identification based on proprioceptive sensor data, not including dynamic state information of a moving robot, have been proposed. As proprioceptive sensors, the vibration information of an accelerometer or IMU and the current information of wheel motors were used to make the data signals, which are transformed into soil feature data in frequency domain using a Fast Fourier Transform (FFT). The soil feature data were classified into one of pre-learned soil models by a support vector machine (SVM) (Brooks et al., 2012, Iagnemma et al., 2005) or a probabilistic neural network (PNN) (Coyle et al., 2008, Ojeda et al., 2006). The performance of identifying a soil type was verified through driving simulations or real driving experiments on rough terrains. However, these algorithms have physical limitations on real applications of wheeled robots. First of all, the vibration and current information is strongly influenced by a robot speed and also a surface shape. Therefore, although two robots move on the same type of soil, it might indicate the result of identifying one into another soil type depending on a robot speed and a surface shape.

With wheel-soil interaction models for planetary rovers on loose soils, the algorithms for soil identification and for optimal wheel control were proposed. In Brooks et al., 2012, the purpose of soil identification is to estimate the maximum traction through optimization of a traction force model, based on observed rover wheel torque and sinkage. And in Iagnemma et al., 2004, the purpose of soil identification is to estimate key soil parameters, cohesion c and internal friction angle ϕ which can be used to compute maximum shear stress related to maximum traction of wheels. To identify distinct type of soil, in these researches, proprioceptive sensor data are needed to be measured or estimated, such as the vertical load, torque, wheel angular speed, wheel linear speed and sinkage. The algorithms were demonstrated using experimental data from a four-wheeled robot in an outdoor Mars-analogue environment. However, these methods cannot be utilized for some wheeled robots like military vehicles which are sometimes operated on hard surfaces such as grass or firm soil, where the sinkage does not occur because the force equations become zero. On loose soils, it is also not easy to be employed since it is difficult to precisely estimate sinkage by vision or distance sensors.

To solve these problems, this paper proposes an algorithm to estimate optimal control parameters; maximum traction coefficient and optimal slip ratio on rough surfaces with various soil types from a hard surface through a loose surface, based on soil strength without estimating wheel sinkage.

2 MODELLING OF OPTIMAL CONTROL PARAMETERS

2.1 Improved Brixius Equation based on Soil Strength

Brixius equation is well-known as one of empirical methods, which express tractive characteristics of bias-ply pneumatic tyres on a variety of soil types in outdoor environments (Brixius, 1987, Tiwari et al., 2010). To meet the purpose of this paper, previous Brixius equation is changed into a function of wheel slip ratio S and soil strength K which can be measured or estimated by on-board sensors in real-time, as shown in (3) – (6). In (1), slip ratio is a key state variable and it is expressed as a function of the linear velocity V_x [m/s] and the circumference velocity ωR_w [m/s].

$$S = \frac{\omega R_w - V_x}{\max(V_x, \omega R_w)} \quad (1)$$

where R_w [m] is the wheel radius and ω [rad/s] is the wheel angular velocity. Soil strength K is also a crucial variable for soil identification. Soil strength K is actually estimated on a real-time system of a robot by an algorithm for soil identification in this paper.

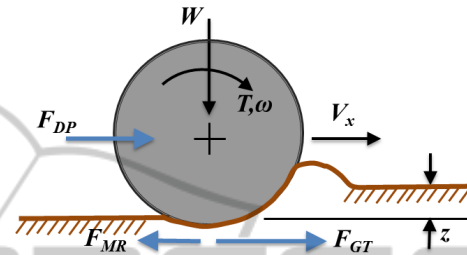


Figure 1: Forces acting on a driving wheel.

Figure 1 shows forces acting on a driving wheel during a wheel-terrain interaction by wheel torque T [Nm] and normal load W [N]. In (2), drawbar pull F_{DP} [N] is expressed by difference of gross traction F_{GT} [N] and motion resistance F_{MR} [N].

$$F_{DP} = F_{GT} - F_{MR} \quad (2)$$

By Brixius equation, gross traction F_{GT} and motion resistance F_{MR} are as follows:

$$F_{GT} = \pm W \left[C_1 (1 - e^{-C_2 K}) (1 - e^{\mp C_3 S}) + C_4 \right] \quad (3)$$

$$F_{MR} = W \left[\left(\frac{C_5}{K} + C_4 \pm \frac{C_6 S}{\sqrt{K}} \right) \right] \quad (4)$$

By (2), drawbar force F_{DP} is defined as:

$$F_{DP} = \pm W \left[C_1 (1 - e^{-C_2 K}) (1 - e^{\mp C_3 S}) - \left(\frac{C_5}{K} \pm \frac{C_6 S}{\sqrt{K}} \right) \right] \quad (5)$$

where C_1 , C_2 , C_3 , C_4 , C_5 , and C_6 are Brixius constants and the values are determined by a nonlinear regression technique. Equation (5) is divided by normal load W as follows: (upper sign: $S > 0$, lower sign: $S < 0$)

$$\mu = \pm \left[C_1 (1 - e^{-C_2 K}) (1 - e^{\mp C_3 S}) - \left(\frac{C_5}{K} \pm \frac{C_6 S}{\sqrt{K}} \right) \right] \quad (6)$$

Equation (6) represents traction – slip curves according to strength of soil K .

2.2 Derivation of OCP Models

For derivation of optimal slip models, indoor

experiments to acquire force data (F_{DP} , F_{GR} , and F_{MR}) in Figure 1 were conducted on three types of soil: sand, gravel and grass where soil strengths are different, as shown in Figure 2. In the system of the testbed, the maximum angular velocity is 4.5 rad/s and the maximum linear velocity is 32 cm/s. Experimental slip conditions were controlled at 0.1, 0.2, 0.3, 0.4, 0.5 and 0.6. From measured data of the testbed, Brixius equation can be completed based on soil strength K of each soil type. Brixius constants in the equations are calculated by a nonlinear regression technique using a statistics program, SPSS as follows: $C_1=1.3$, $C_2=0.01$, $C_3=7.058$, $C_4=0.04$, $C_5=-5$, $C_6=4$. Strength of soils K are also given: 50 (sand), 80 (gravel) and 200 (grass), respectively.

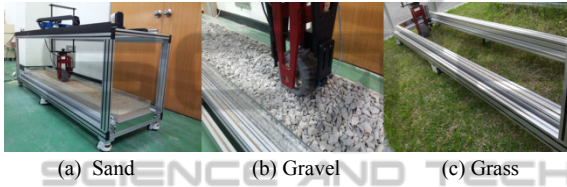


Figure 2: Wheel-soil interaction experiments using a testbed on three types of soil.

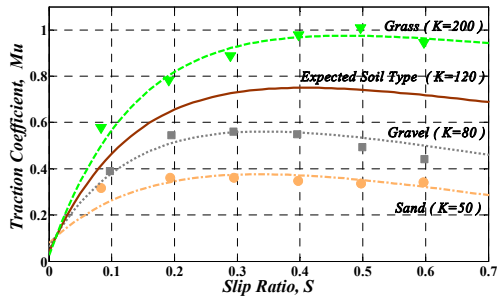


Figure 3: Traction-slip curve on soil types; sand, gravel and grass.

Using the given Brixius constants and soil strengths, graphs of relation between wheel traction and slip were drawn about the four types of soil from (6), as shown in Figure 3. Actually, a curve in between grass and gravel was not acquired from the indoor experiments. When watching the gap between the curves, it is possible to expect that there exists another soil type which is harder than gravel or softer than grass. The expected soil type (EST) seems to have soil strength of $K=120$. On all the curves, wheel traction is changed by increasing wheel slip. And wheel traction indicates that it has the maximum value at peak points on the curves having a particular slip ratio. In this paper, the point is named optimal slip ratio for maximum traction, S_T . And S_T points can be calculated by partially

differentiating the traction-slip equation (6) with respect to slip ratio S . Therefore the optimal slip model for maximum traction and also the maximum

$$S_T = \ln \left(\frac{C_6}{C_1 C_3 \sqrt{K} (1 - e^{-C_2 K})} \right)^{\frac{1}{C_3}} \quad (7)$$

$$\mu_T = \pm \left[C_1 (1 - e^{-C_2 K}) (1 - e^{\mp C_3 S_T}) - \left(\frac{C_5}{K} \pm \frac{C_6 S_T}{\sqrt{K}} \right) \right] \quad (8)$$

traction coefficient model are defined as functions of soil strength K by (7) and (8), respectively.

In another case, Brixius equations can be employed for analysis of wheel tractive efficiency of (9). Equation (9) represents the degree of generated drawbar pull F_{DP} when gross traction F_{GT} acts on wheels. From Brixius equation (3) and (5), the curves of tractive efficiency are described as shown in Figure 4. All tractive efficiency on soil types increases rapidly until reaching peak points near 0.1 of the slip ratio and decreases dramatically after that. In this paper, the slip ratio is called optimal slip ratio for TE , S_E and it means that wheeled robots can minimize energy consumption if the robots keep wheel slip at S_E while moving on rough terrains.

$$TE = \frac{\text{Output power}}{\text{Input power}} = \frac{F_{DP}}{F_{GT}} (1 - S) \quad (9)$$

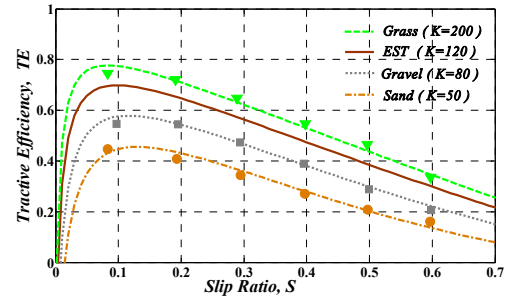


Figure 4: Tractive efficiency on soil types; sand, gravel and grass.

To derive an optimal slip model for maximum TE , it is possible to partially differentiate the TE equation (9) with respect to slip ratio S . However, there is complexity for partial differentiation of (9) where the nonlinear equation (3) and (5) are included. For simplification, the S_E model is derived as a linear equation of soil strength K from real peak points on each curve on the basis that the points of maximum TE move on the curves at near 0.1 of slip ratios. Derived S_E model is as follows:

$$S_E = \frac{(K - \alpha)}{\beta}, \quad \alpha = 677.4, \quad \beta = -5242.9 \quad (10)$$

As an example, Figure 5 describes optimal values; maximum traction coefficient μ_T , optimal slip ratio for traction S_T and for TE S_E calculated from the optimal control parameter (OCP) models based on the soil strength $K=120$. Derived OCP models include a wide range of soil types from a hard surface like asphalt through a loose surface like sand. Once soil strength K is estimated in the range from zero to infinity, optimal control parameters are determined and used to optimally adjust wheel rotations according to the control purpose.

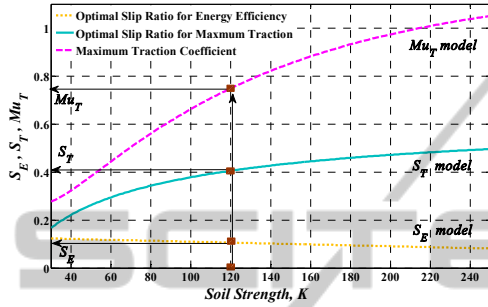


Figure 5: OCP curves depending on soil strength K .

3 PROPRIOCEPTIVE ESTIMATION OF SOIL STRENGTH

In this section, a method for estimation of soil strength K was suggested. Soil strength K can be simply determined through observing actual traction coefficient μ and slip ratio S on the traction-slip curve as shown in Figure 3. The estimator of the actual traction coefficient is developed based on wheeled robot dynamic models. Actual slip ratios of wheels can be calculated by (1). Acquired real information of the traction coefficient and the slip ratio are employed to estimate soil strength K on the traction-slip curve in Figure 3 by a numerical method.

3.1 Estimation of Real Traction Coefficient

The real traction coefficient estimator developed in this paper, which does not cause a huge computational burden or require derivations of sensor signals, is based on a Kalman filter using wheeled robot dynamics shown in Figure 6. The motion equation of the robot on the X_R - Y_R - Z_R robot coordinates described in Figure 6 is

$$I_z \dot{\psi} = d(F_{x_3} + F_{x_4}) - c(F_{x_1} + F_{x_2}) - M_{z,R} \quad (11)$$

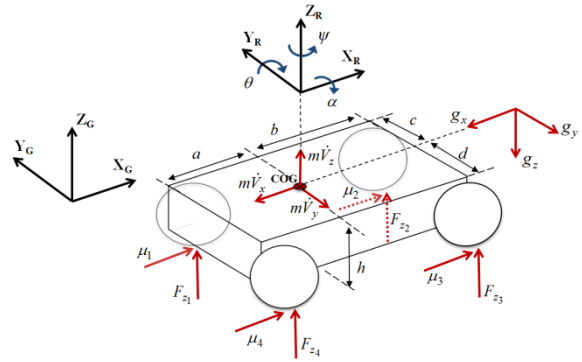


Figure 6: Four-wheel drive, differentially steered robot.

where ψ is the yaw rate; I_z represents the moment of inertia of the robot, a and b are the distances from the center of mass of the robot to the rear axle and the front axle, respectively. And $M_{z,R}$ is the resistance moment about Z_R -axis and it is defined as:

$$M_{z,R} = a(\mu_{y,R_1} F_{z_1} + \mu_{y,R_4} F_{z_4}) + b(\mu_{y,R_2} F_{z_2} + \mu_{y,R_3} F_{z_3}) \quad (12)$$

where $\mu_{y,R}$ is the lateral motion resistance coefficient on Y_R -axis and F_z is the normal forces on wheels. The subscript i indicates that 1 is the left-rear wheel, 2 is the left-front wheel, 3 is the right-front wheel and 4 is the right-rear wheel.

The motion equation for the wheel is as follows:

$$I_\omega \dot{\omega}_i = T_i - R_w F_{x_i} - R_w F_{x,R_i} \quad (13)$$

where T is the wheel torque, I_ω is the moment of inertial of a wheel, F_x and $F_{x,R}$ are the longitudinal traction and the motion resistance on X_R -axis, which can be obtained as follows:

$$F_{x_i} = \mu_i F_{z_i} \quad (14)$$

$$F_{x,R_i} = \mu_{x,R_i} F_{z_i} \quad (15)$$

where μ is the longitudinal traction coefficient on wheels and $\mu_{x,R}$ is the motion resistance coefficient on X_R -axis. In (11)-(14), the normal force F_z is calculated by 3-dimentional normal force dynamics defined as:

$$F_{z_2}(a+b) + F_{z_3}(a+b+c+d) + F_{z_4}(c+d) = -m\dot{V}_x h + m\dot{V}_y h + m\dot{V}_z(a+c) - mg_x h + mg_y h + mg_z(a+c) \quad (16)$$

$$F_{z_1}(a+b) + F_{z_3}(c+d) + F_{z_4}(a+b+c+d) = m\dot{V}_x h + m\dot{V}_y h + m\dot{V}_z(b+c) + mg_x h + mg_y h + mg_z(b+c) \quad (17)$$

$$F_{z_1}(a+b+c+d) + F_{z_2}(c+d) + F_{z_4}(a+b) = m\dot{V}_x h - m\dot{V}_y h + m\dot{V}_z(b+d) + mg_x h - mg_y h + mg_z(b+d) \quad (18)$$

$$F_{z_1}(c+d) + F_{z_2}(a+b+c+d) + F_{z_3}(a+b) = -m\dot{V}_x h - m\dot{V}_y h + m\dot{V}_z(a+d) - mg_x h - mg_y h + mg_z(a+d) \quad (19)$$

where m is the robot mass; h is the height from the surface to the center of mass of the robot; c and d are the distances from the center of mass of the robot to the left wheels and the right wheels; \dot{V}_x , \dot{V}_y and \dot{V}_z are the acceleration; g_x , g_y and g_z are the gravity force on the X_R - Y_R - Z_R robot coordinates, respectively. The gravity force is defined by (20)

$$\mathbf{G}_R = \mathbf{R}_x^T \mathbf{R}_y^T \mathbf{G}_G = \begin{bmatrix} g_x \\ g_y \\ g_z \end{bmatrix} = \begin{bmatrix} 1 & 0 & 0 \\ 0 & c\alpha & -s\alpha \\ 0 & s\alpha & c\alpha \end{bmatrix}^T \begin{bmatrix} c\theta & 0 & s\theta \\ 0 & 1 & 0 \\ -s\theta & 0 & c\theta \end{bmatrix}^T \begin{bmatrix} 0 \\ 0 \\ g_G \end{bmatrix} = \begin{bmatrix} -g_G s\theta \\ g_G s\alpha c\theta \\ g_G c\alpha c\theta \end{bmatrix} \quad (20)$$

where \mathbf{R}_x and \mathbf{R}_y are the rotation matrices about X_G and Y_G -axis, \mathbf{G}_G is the gravity force vector on the global coordinate system. From (16)-(19), the equations are transformed into a form of a matrix as follows:

$$\mathbf{B} = \mathbf{A}\mathbf{F}_z \quad (21)$$

where

$$\mathbf{F}_z = \begin{bmatrix} F_{z1} & F_{z2} & F_{z3} & F_{z4} \end{bmatrix}^T \quad (22)$$

$$\mathbf{A} = \begin{bmatrix} 0 & a+b & a+b+c+d & c+d \\ a+b & 0 & c+d & a+b+c+d \\ a+b+c+d & c+d & 0 & a+b \\ c+d & a+b+c+d & a+b & 0 \end{bmatrix} \quad (23)$$

$$\mathbf{B} = \begin{bmatrix} -m\dot{V}_x h + m\dot{V}_y h + m\dot{V}_z(a+c) - mg_x h + mg_y h + mg_z(a+c) \\ m\dot{V}_x h + m\dot{V}_y h + m\dot{V}_z(b+c) + mg_x h + mg_y h + mg_z(b+c) \\ m\dot{V}_x h - m\dot{V}_y h + m\dot{V}_z(b+d) + mg_x h - mg_y h + mg_z(b+d) \\ -m\dot{V}_x h - m\dot{V}_y h + m\dot{V}_z(a+d) - mg_x h - mg_y h + mg_z(a+d) \end{bmatrix} \quad (24)$$

The normal forces are calculated by (25) defined as:

$$\mathbf{F}_z = \mathbf{A}^{-1}\mathbf{B} \quad (25)$$

From (11)-(15), the states for the Kalman filter are defined as follows:

$$\mathbf{x}(t) = [\boldsymbol{\mu} \quad \boldsymbol{\mu}_{x,R} \quad \boldsymbol{\mu}_{y,R} \quad \boldsymbol{\psi} \quad \boldsymbol{\omega}]^T \quad (26)$$

where

$$\boldsymbol{\mu} = [\mu_1 \quad \mu_2 \quad \mu_3 \quad \mu_4] \quad (27)$$

$$\boldsymbol{\mu}_{x,R} = [\mu_{x,R1} \quad \mu_{x,R2} \quad \mu_{x,R3} \quad \mu_{x,R4}]$$

$$\boldsymbol{\mu}_{y,R} = [\mu_{y,R1} \quad \mu_{y,R2} \quad \mu_{y,R3} \quad \mu_{y,R4}]$$

$$\boldsymbol{\omega} = [\omega_1 \quad \omega_2 \quad \omega_3 \quad \omega_4]$$

The measurements are

$$\mathbf{z}(t) = [\dot{V}_x \quad \boldsymbol{\psi} \quad \omega_1 \quad \omega_2 \quad \omega_3 \quad \omega_4]^T \quad (28)$$

where

$$\dot{V}_x = \frac{1}{m}(F_{x1} + F_{x2} + F_{x3} + F_{x4}) = \frac{1}{m}(\mu_1 F_{z1} + \mu_2 F_{z2} + \mu_3 F_{z3} + \mu_4 F_{z4}) \quad (29)$$

Equations (11)-(15) and (26)-(29) are integrated to build the following state-space system with process noise $\mathbf{w}(t)$ and measurement noise $\mathbf{v}(t)$ as follows:

$$\dot{\mathbf{x}}(t) = \mathbf{A}(t)\mathbf{x}(t) + \mathbf{B}(t) + \mathbf{w}(t) \quad (33)$$

$$\mathbf{z}(t) = \mathbf{H}(t)\mathbf{x}(t) + \mathbf{v}(t)$$

where $\mathbf{A}(t)$, $\mathbf{B}(t)$ and $\mathbf{H}(t)$ are defined in (30)-(32), and their $\mathbf{I}_{i \times k}$ and $\mathbf{O}_{i \times k}$ denote an $i \times k$ identity matrix and a zero matrix, respectively. Equation (33) is discretized using zero-order hold for being applicable to the discrete-time Kalman filter as follows:

$$\mathbf{x}_{k+1} = \mathbf{A}_k \mathbf{x}_k + \mathbf{B}_k + \mathbf{w}_k \quad (34)$$

$$\mathbf{z}_k = \mathbf{H}_k \mathbf{x}_k + \mathbf{v}_k$$

The algorithm of the discrete-time Kalman filter is

$$\bar{\mathbf{x}}_{k+1} = \mathbf{A}_k \hat{\mathbf{x}}_k + \mathbf{B}_k$$

$$\mathbf{M}_{k+1} = \mathbf{A}_k \mathbf{P}_k \mathbf{A}_k^T + \mathbf{W}_k \quad (35)$$

$$\hat{\mathbf{x}}_{k+1} = \bar{\mathbf{x}}_{k+1} + \mathbf{P}_k \mathbf{H}_k^T \mathbf{V}_k^{-1} (\mathbf{z}_k - \mathbf{H}_k \bar{\mathbf{x}}_k)$$

$$\mathbf{P}_k = \mathbf{M}_k - \mathbf{M}_k \mathbf{H}_k^T [\mathbf{H}_k \mathbf{M}_k \mathbf{H}_k^T + \mathbf{V}_k]^{-1} \mathbf{H}_k \mathbf{M}_k$$

where \mathbf{W}_k and \mathbf{V}_k represent the covariance matrices of $\mathbf{w}(t)$ and $\mathbf{v}(t)$. The estimator includes the motion equations for the wheeled robot, but the traction coefficients μ_i are considered to be unknown parameters to be estimated. And also, the longitudinal motion resistance coefficients $\mu_{x,Ri}$ are included in the estimator in order to observe the change of surface shapes and of soil types.

3.2 Estimation of Soil Strength by Numerical Method

From derived actual traction coefficient and slip ratio, soil strength K is simply estimated by a numerical method. The numerical update rule of soil strength K is defined as:

$$K_{n+1} = K_n + \lambda \eta_E \quad (36)$$

where K_{n+1} is the updated value of soil strength; K_n is the previous value of soil strength, λ is the learning rate selected in the range between 1 and 0, η_E is the learning weight defined as:

$$\eta_E = \left| \frac{\mu_{ref}}{S_a} - \frac{\mu_e}{S_a} \right| = \left| \frac{E}{S_a} \right| \quad (37)$$

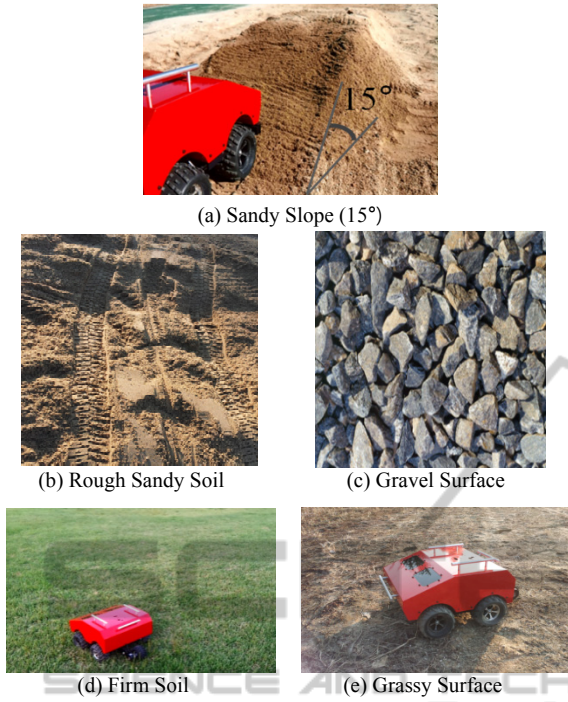


Figure 7: Experimental terrain types.

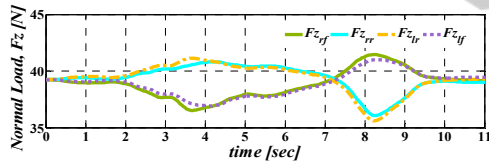


Figure 8: Estimated normal forces on the sandy slope.

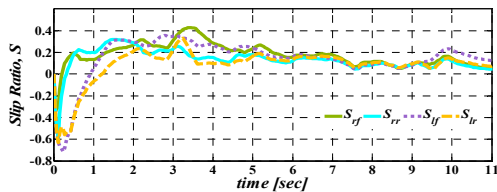


Figure 9: Estimated slip ratios on the sandy slope.

and actual slip ratio, soil strength K on the sandy slope was estimated by the numerical method as shown in Figure 12 and 13. The convergence time was average 0.01 seconds every samples. Figure 12 displays the flow of soil strength K in the vicinity of the desired area of soil strength of sand in contrast with Figure 13. In Figure 13, the estimated soil strength is gradually decreasing during the whole time. From these results in Figure 12 and Figure 13, it can be verified that the suggested algorithm improves the performance of soil identification. Figure 14 describes the results of estimating optimal control parameters from the estimated soil strength

on the sandy slope. Actually, the pre-experimental data were placed on about $K=50$, $\mu_T=0.4$, $S_T=0.26$ and $S_E=0.12$. In Figure 14, it is considered that the outdoor experimental sandy surface had more moisture, in that time, than the indoor experimental sand surface though the estimated optimal control parameters indicates slightly higher values than the pre-experimental data.

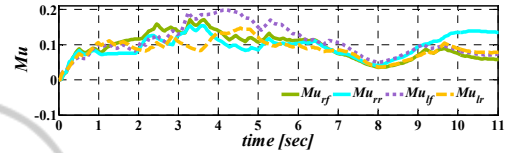
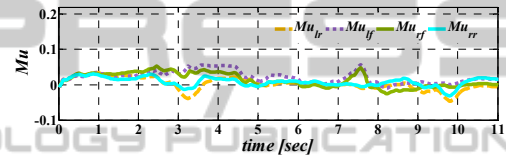
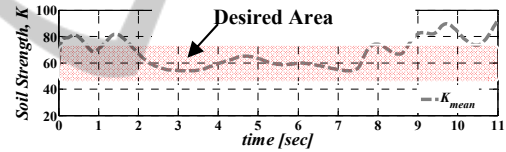
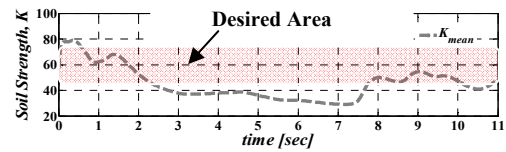
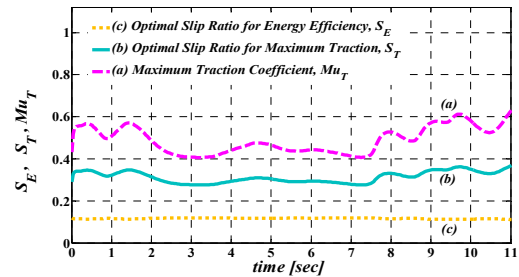

 Figure 10: Estimated traction coefficient μ with compensating motion resistance on the sandy slope.

 Figure 11: Estimated traction coefficient μ without compensating motion resistance on the sandy slope.

 Figure 12: Estimated soil strength K with compensating motion resistance on the sandy slope.

 Figure 13: Estimated soil strength K without compensating motion resistance on the sandy slope.


Figure 14: Estimated optimal control parameters on the sandy slope.

As other driving experiments at robot speed 1 m/s on the four types of soil in Figure 7 (b)–(e), Figure 15 describes the results of estimating soil strength K depending on soil types. From 0 to 1 second, there are error values by the initial measurement errors of wheel slip since the slip ratio is very sensitive when the robot moves at low speed.

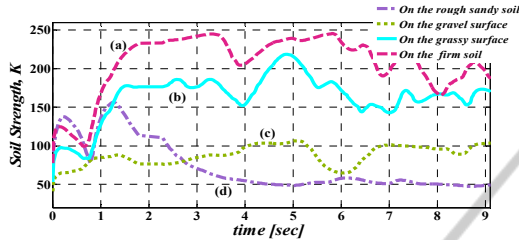


Figure 15: Estimated soil strength K on (a) firm soil (b) grassy surface (c) gravel surface (d) rough sandy soil.

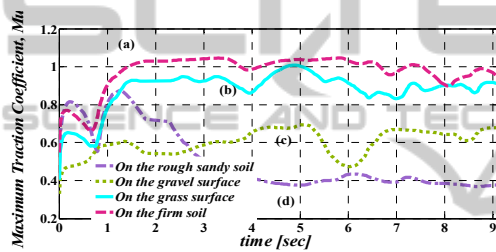


Figure 16: Estimated maximum traction coefficient μ_T on (a) firm soil (b) grassy surface (c) gravel surface (d) rough sandy soil.

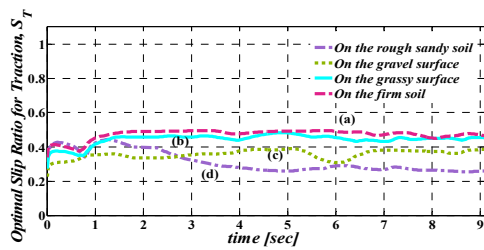


Figure 17: Estimated optimal slip ratio for traction S_T on (a) firm soil (b) grassy surface (c) gravel surface (d) rough sandy soil.

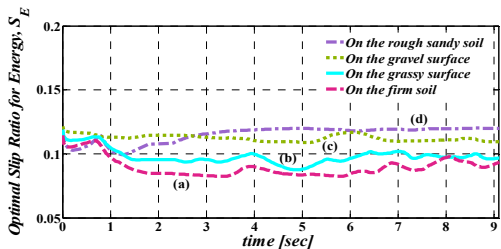


Figure 18: Estimated optimal slip ratio for energy S_E on (a) firm soil (b) grassy surface (c) gravel surface (d) rough sandy soil.

5 CONCLUSION

This paper proposed an algorithm for acquiring optimal control parameters, such as maximum traction coefficient and optimal slip ratio to maximize traction or minimize energy consumption, based on estimating strength of soils. In this paper the optimal models for wheel traction and slip were derived through indoor experiments using a testbed for analysis of wheel-terrain interactions on three types of soil; grass, gravel and sand. For estimating soil strength, actual traction coefficient, including information of motion resistance, was observed by the DKF-based state estimator related to wheeled robot dynamics. The actual traction coefficient and slip ratio on wheels were employed to estimate soil strength by the numerical method on the basis on derived optimal models. The proposed algorithm was verified through real driving experiments of the wheeled robot on various types of soil. From the evaluation of the estimation results, it could confirm that the suggested algorithm has enough performance to identify soil types on rough terrains.

ACKNOWLEDGEMENTS

The Authors gratefully acknowledge the support from UTRC (Unmanned Technology Research Center) at KAIST (Korea Advanced Institute of Science and Technology), originally funded by DAPA, ADD

REFERENCES

Jared D. Terry and Mark A. Minor, 2008, Traction Estimation and Control for Mobile Robots using the Wheel Slip Velocity, *IEEE/RSJ International Conference on Intelligent Robots and Systems*.
 Ambrose Krebs, Fabian Risch, Thomas Thueer, Jerome Maye, Cedric Pradalier and Roland Siegwart, 2010, Rover control based on an optimal torque distribution – Application to 6 motorized wheels passive rover, *IEEE/RSJ International Conference on Intelligent Robots and Systems*.
 Sang Hyun Joo, Jeong Han Lee, Yong Woon Park, Wand Suk Yoo and Jihong Lee, 2013, Real time traversability analysis to enhance rough terrain navigation for an 6x6 autonomous vehicle, *Journal of Mechanical Science and Technology*, Vol. 4, No. 27, pp. 1125-1134.
 Liang Ding, Haibo Gao, Zongquan Deng and Zhen Liu, 2010, Slip-Ratio-Coordinated Control of Planetary Exploration Robots Traversing over Deformable

- Rough Terrain”, *IEEE/RSJ International Conference on Intelligent Robots and Systems*.
- Genya Ishigami, Keiji Nagatani and Kazuya Yoshida, 2008, Slope Traversal Experiments with Slip Compensation Control for Lunar/Planetary Exploration Rover, *IEEE International Conference on Robotics and Automation*.
- C. A Brooks and K. Iagnemma, 2012, Self-Supervised Terrain Classification for Planetary Surface Exploration Rovers, *Journal of Field Robotics*, vol. 29, no. 1.
- C. A Brooks and K. Iagnemma, 2005, Vibration-based terrain classification for planetary exploration rovers, *IEEE Transactions on Robotics*, 21(6), 1185–1191.
- E. J. Coyle and E. G. Collins, 2008, Vibration-Based Terrain Classification Using Surface Profile Input Frequency Responses, *IEEE International Conference on Robotics and Automation*.
- L. Ojeda, J. Borenstein, G. Witus, and R. Karlsen, , 2006, Terrain and Classification with a Mobile Robot,” *Journal of Field Characterization Robotics*, vol. 23, no. 2.
- K. Iagnemma and S. Dubowsky, 2004, Mobile robots in rough terrain: estimation, motion planning and control with application to planetary rover,” *Springer Tracts in Advanced Robotics 12*. Berlin: Springer.
- W. W. Brixius, 1987, Traction prediction equations for bias ply tires, *ASAE*, no. 87-1622.
- V. K. Tiwari, K. P. Pandey, and P. K. Pranav, 2010, A review on traction prediction equations, *Journal of Terramechanics*, vol. 47, pp. 191-199.